

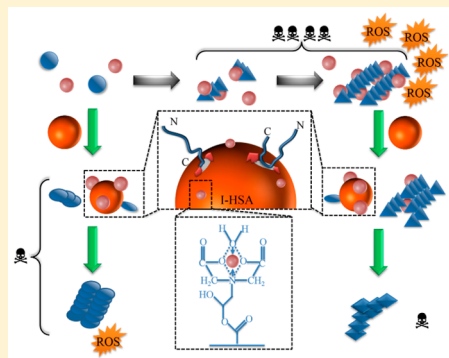
Iminodiacetic Acid-Modified Human Serum Albumin: A Multifunctional Agent against Metal-Associated Amyloid β -Protein Aggregation and Cytotoxicity

Baolong Xie, Huan Zhang, Xi Li, Xiaoyan Dong,[✉] and Yan Sun[✉]

Department of Biochemical Engineering and Key Laboratory of Systems Bioengineering of the Ministry of Education, School of Chemical Engineering and Technology, Tianjin University, Tianjin 300354, China

Supporting Information

ABSTRACT: Metal-induced amyloid β -protein ($A\beta$) aggregation plays a key role in the pathogenesis of Alzheimer's disease. Although several agents have been recognized to block metal-associated $A\beta$ aggregation, their therapeutic potential is marred due to the high-concentration metal ions in the amyloid plaques. To overcome this problem, we have herein developed iminodiacetic acid-modified human serum albumin (I-HSA) to fight against the aggregation. The multifunctional nature of I-HSA was extensively characterized in inhibiting the $A\beta_{42}$ aggregation associated with Zn^{2+} and Cu^{2+} . The results revealed the following: (1) I-HSA significantly inhibited $A\beta_{42}$ aggregation and alleviated its cytotoxicity. (2) I-HSA possessed a metal-chelate capacity as high as 31.2 mol/mol, and 25 μ M I-HSA could effectively inhibit the influence of 250 μ M Zn^{2+} on $A\beta_{42}$ aggregation. (3) Equimolar I-HSA remarkably attenuated the reactive oxygen species damage caused by the $A\beta_{42}$ and $Cu^{2+}-A\beta_{42}$ species. (4) I-HSA could remodel metal- $A\beta_{42}$ fibrils into unstructured aggregates with less neurotoxicity. The cytotoxicity of mature $Cu^{2+}-A\beta_{42}$ aggregates was mitigated from 64.8% to 25.4% under the functioning of I-HSA. In conclusion, I-HSA showed prominent advantages for the high metal-chelate capacity. To our knowledge, I-HSA is the first multifunctional macromolecule for inhibiting high-concentration metal-induced $A\beta_{42}$ aggregation and remodeling mature metal-induced $A\beta_{42}$ species.



KEYWORDS: Amyloid β -protein, Metal chelator, Inhibition, Surface modification, Aggregation, Multifunctionality

INTRODUCTION

Alzheimer's disease (AD) is a kind of chronic neurodegenerative disorder causing memory decline and dysfunction of cognitive functions.^{1–3} Pathologically, the presence of progressive amyloid plaques in brain tissues is believed to be the main hallmark associated with AD.^{4–6} The amyloid plaques are primarily composed of aggregates of amyloid β -proteins ($A\beta$). Although the precise neurotoxic mechanism remains controversial, pathological and genetic evidence strongly support that $A\beta$ aggregation is the central process leading to AD.⁷ Therefore, inhibition of $A\beta$ aggregation is considered as an effective strategy for the treatment of AD.

Moreover, recent research advances have revealed the presence of high-concentration transition-metal ions, such as Zn^{2+} and Cu^{2+} as high as 1100 and 400 μ M, respectively, in the amyloid plaques, which make amyloid clearance more problematic.^{8,9} It has been proven that the metal ions facilitate the formation of unstructured aggregates rather than amyloid fibrils with β -sheet structures.^{10,11} In addition to the kinetic effects, the redox effects of the metal ions contribute to the generation of neurotoxic reactive oxygen species (ROS), especially for Cu^{2+} , which could cause severe oxidative stress and cell damage.^{12,13}

In order to remove the harmful effects of the metal-ion-associated $A\beta$ aggregation and cytotoxicity, many metal chelators targeting metal- $A\beta$ species have been studied, such as ethylenediaminetetraacetic acid disodium salt, clioquinol (CQ), and derivatives of CQ (PBT2).^{14,15} In phase II clinical trials, CQ and PBT2 have proven to improve the cognitive performance and memory of AD patients due to the ability of CQ and PBT2 to inhibit the binding of metal ions to $A\beta$.^{15,16} However, these agents exposed limitations in their poor biocompatibility and bioavailability.¹⁷ More seriously, large dosages of the agents are required in the treatment to overcome the high-concentration metal ions in amyloid plaques, which might lead to toxic side-effects.¹⁸ Moreover, the chelators have an inappreciable inhibitory effect on $A\beta$ aggregation. Hence, there is an urgent demand for the development of biocompatible multifunctional agents that possess a potent inhibition effect on $A\beta$ aggregation and the generation of ROS, a high metal-chelate capacity, and a high efficiency for remodeling mature metal-induced $A\beta$ species.

Received: April 6, 2017

Accepted: August 2, 2017

Published: August 2, 2017

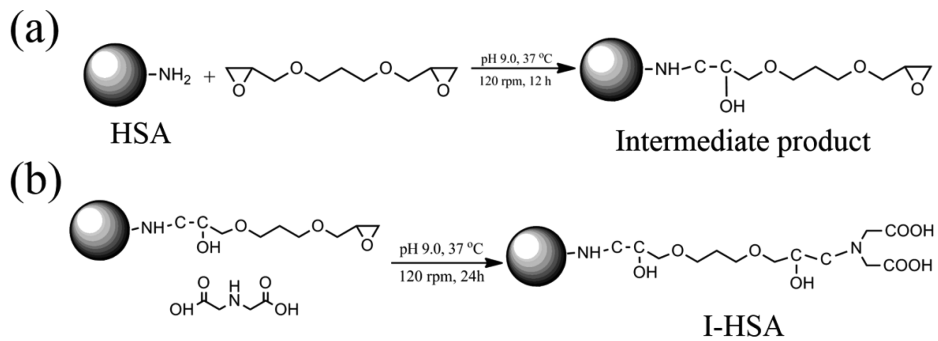
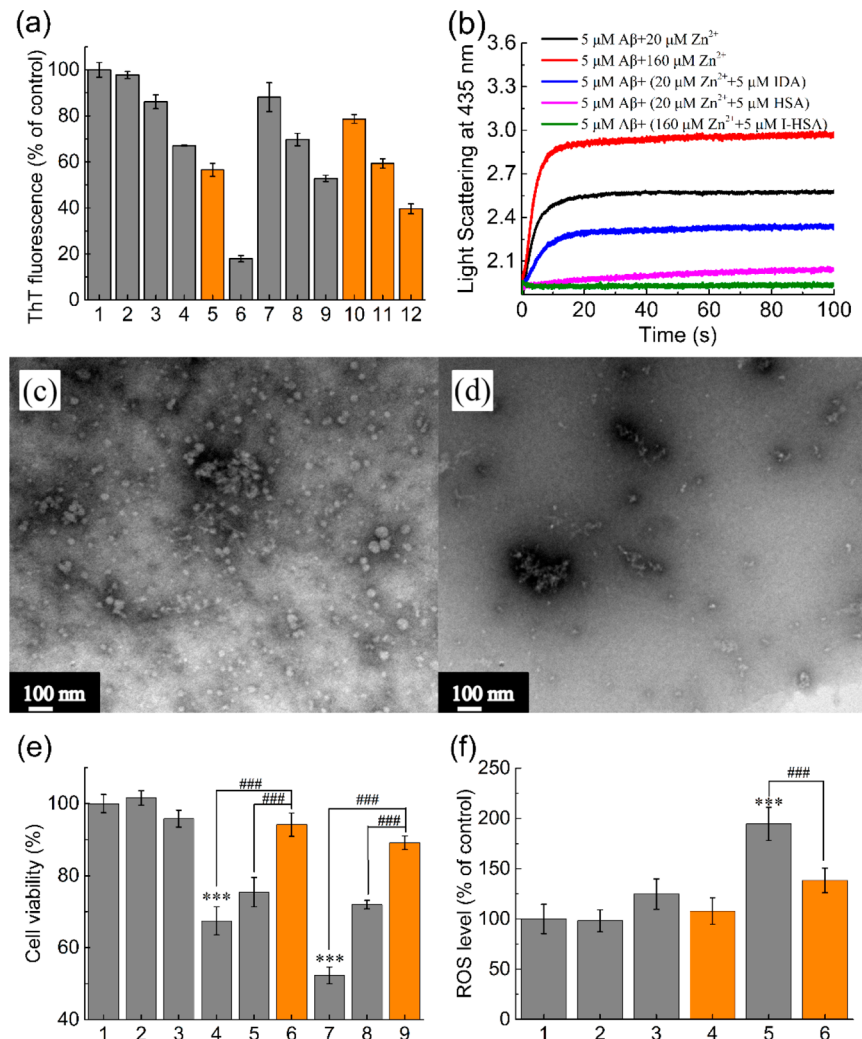
**Figure 1.** Reaction scheme for the modification of HSA.

Figure 2. Inhibition of metal-mediated $\text{A}\beta_{42}$ aggregation and reduction of metal- $\text{A}\beta_{42}$ cytotoxicity by I-HSA. (a) Normalized ThT fluorescence intensities for the inhibition of $\text{A}\beta_{42}$ aggregation for 24 h. Lanes denote the following conditions: 1, $\text{A}\beta_{42}$ alone; 2, $\text{A}\beta_{42}$ + IDA; 3, $\text{A}\beta_{42}$ + HSA; 4, $\text{A}\beta_{42}$ + A-HSA; 5, $\text{A}\beta_{42}$ + I-HSA; 6, $\text{A}\beta_{42}$ + Zn^{2+} ; 7, $\text{A}\beta_{42}$ + Zn^{2+} + IDA; 8, $\text{A}\beta_{42}$ + Zn^{2+} + HSA; 9, $\text{A}\beta_{42}$ + Zn^{2+} + A-HSA; 10, $\text{A}\beta_{42}$ + Zn^{2+} + 2.5 μM I-HSA; 11, $\text{A}\beta_{42}$ + Zn^{2+} + 12.5 μM I-HSA; 12, $\text{A}\beta_{42}$ + Zn^{2+} + 25 μM I-HSA. The final concentrations of $\text{A}\beta_{42}$, IDA, HSA, and Zn^{2+} were all 25 μM unless stated otherwise. (b) Kinetic traces followed by stopped-flow fluorescence of Zn^{2+} binding to $\text{A}\beta_{42}$ with or without HSA/I-HSA/IDA. Samples are as indicated in the legend. (c) TEM images of $\text{A}\beta_{42}$ in the presence of equimolar Zn^{2+} after 24 h incubation. (d) TEM images of $\text{A}\beta_{42}$ in the presence of equimolar Zn^{2+} and I-HSA after 24 h incubation. (e) The viability of SH-SY5Y cells incubated with Lane 1, buffer A (20 mM 2-[4-(2-hydroxyethyl)-1-piperazine] ethanesulfonic acid (HEPES), 100 mM NaCl, pH 7.4); Lane 2, I-HSA; Lane 3, Zn^{2+} ; Lane 4, $\text{A}\beta_{42}$ fibrils; Lane 5, HSA-mediated $\text{A}\beta_{42}$ fibrils; Lane 6, I-HSA-mediated $\text{A}\beta_{42}$ fibrils; Lane 7, Zn^{2+} - $\text{A}\beta_{42}$ aggregates; Lane 8, HSA-mediated Zn^{2+} - $\text{A}\beta_{42}$ aggregates; Lane 9, I-HSA-mediated Zn^{2+} - $\text{A}\beta_{42}$ aggregates. The final concentrations of $\text{A}\beta_{42}$, HSA, I-HSA, and Zn^{2+} were all 25 μM . (f) ROS level in SH-SY5Y cells upon treatment with different samples. Lane 1, control with buffer B (20 mM HEPES, 100 mM NaCl, pH 6.6); Lane 2, I-HSA; Lane 3, $\text{A}\beta_{42}$ fibrils; Lane 4, I-HSA-mediated $\text{A}\beta_{42}$ aggregates; Lane 5, Cu^{2+} - $\text{A}\beta_{42}$ aggregates; Lane 6, I-HSA-mediated Cu^{2+} - $\text{A}\beta_{42}$ aggregates. The final concentrations of $\text{A}\beta_{42}$, I-HSA, and Cu^{2+} were all 25 μM . ***, $p < 0.001$ as compared to Lane 1. The values of $p < 0.001$ for the pairs of data sets are marked with ***.

Currently, it is a prevalent method to conjugate metal chelators onto proteins or nanoparticles to increase their biocompatibility and their ability to inhibit metal-associated $\text{A}\beta$ aggregation.¹⁹ Among the various proteins/nanoparticles, human serum albumin (HSA) is a natural inhibitor against $\text{A}\beta$ aggregation *in vivo*^{20,21} and plays an important role in the transportation of metal ions in blood plasma.^{22,23} Also, HSA has considerable pharmaceutical utility for its physicochemical stability and biocompatibility.^{24–26} However, the metal-chelate capacity of HSA is very limited, making it unable to deal with the high-concentration metal ions in the brain tissues of AD patients.²⁷ Hence, we have focused on the use of HSA to develop potent inhibitors of $\text{A}\beta$ aggregation. Previously, we have proven that the extra negative charges on an acidulated HSA (A-HSA) surface aided the inhibitory effects of $\text{A}\beta$ aggregation more than native HSA.^{27,28} On the basis of these findings, we have herein developed iminodiacetic acid (IDA)-modified HSA (I-HSA), which is expected to offer a high metal-chelate capacity and anti-ROS activity in addition to the potent inhibitory effect of HSA. This article describes our extensive characterization and analysis on the inhibition and remodeling capabilities of I-HSA on $\text{Zn}^{2+}/\text{Cu}^{2+}$ -mediated $\text{A}\beta_{42}$ aggregation and cytotoxicity. The modulation mechanism of I-HSA was explored to advance the knowledge required for further development of multifunctional agents against AD.

RESULTS AND DISCUSSION

Characteristics of I-HSA. Figure 1 shows the two-step reaction for the modification of HSA, and the results are listed in Table S1. It is seen from the table that the two reactions successively increased the molecular weight (MW) of modified HSA to 75 053.4 Da (intermediate product) and 79 199.9 Da (I-HSA), indicating that the modification of IDA increased the MW by 4146.5 Da. The average modification degree of IDA on I-HSA was then calculated to be 31.2 because coupling one IDA molecule increased the MW by 133.1 Da (Figure 1). Moreover, as listed in Table S1, I-HSA (-9.8 ± 0.7 mv) showed a lower zeta-potential value than native HSA (-5.7 ± 0.4 mv). This indicates that the modification decreased the zeta potential of HSA for the conversion of about 31 amino groups into carboxyl groups of IDA. Despite the significant changes of the physicochemical properties of I-HSA from HSA, the modification resulted in an inappreciable change in the molecular size, intrinsic fluorescence spectra, and far-UV circular dichroism spectra of HSA, as shown in Table S1 and Figure S1. This confirms that I-HSA was unchanged in regard to its secondary and tertiary structures.

I-HSA Potently Inhibits Metal-Mediated $\text{A}\beta_{42}$ Aggregation. To evaluate the content of β -sheet structures in $\text{A}\beta_{42}$ aggregates and the inhibition effect of I-HSA against metal-mediated $\text{A}\beta_{42}$ aggregation, Thioflavin T (ThT) fluorescence assays were conducted.²⁹ As reported previously, $\text{A}\beta_{42}$ aggregation reached a steady state by 24 h of incubation.^{27,28} Hence, the fluorescence signals of $\text{A}\beta_{42}$ aggregates at 24 h of incubation are presented for comparison (Figure 2a). It can be seen that the ThT fluorescence intensity with IDA was almost the same as that of the sample of $\text{A}\beta_{42}$ alone, indicating that IDA has an inappreciable effect on $\text{A}\beta_{42}$ aggregation. By contrast, equimolar HSA, A-HSA, and I-HSA obviously decreased the ThT intensities of the self-aggregates of $\text{A}\beta_{42}$ to 86.1, 67.1, and 56.5%, respectively, implying that they could inhibit the amyloid self-aggregation (Figure 2a, Lanes 3–5). Remarkably, the potency of I-HSA under physiological

conditions was much stronger than that of both native HSA and A-HSA designed in our previous work (Figure 2a, Lanes 3–5).^{27,28} The favorable result suggests that the carboxyl groups on the I-HSA surface contributed to the prominent inhibition activity by the hydrophobic binding-electrostatic repulsion (HyBER) mechanism proposed previously.^{27,28} In addition, Zn^{2+} obviously reduced the ThT intensity of $\text{A}\beta_{42}$ fibrils to 17.9% (Figure 2a, Lane 6) due to the formation of spherical aggregates with a small β -sheet structure,^{27,30} which was also confirmed by transmission electron microscopy (TEM) to be discussed below. It is seen from Lane 7 (Figure 2a) that IDA increased the ThT fluorescent signal to 88.1% by chelating Zn^{2+} and diminishing the effect of Zn^{2+} on $\text{A}\beta_{42}$ aggregation. Moreover, the addition of 2.5 μM I-HSA resulted in a significant increase of ThT intensity of $\text{Zn}^{2+}-\text{A}\beta_{42}$ aggregates (Figure 2a, Lane 10). This demonstrated that I-HSA at a low concentration (2.5 μM) could inhibit Zn^{2+} -induced aggregation by chelating a majority of Zn^{2+} , while its inhibition effect on $\text{A}\beta_{42}$ was limited. When more I-HSA was added, the ThT intensity decreased with its concentrations (Figure 2a, Lanes 10–12). This was because I-HSA at higher concentrations could significantly inhibit the formation of β -sheet structures after almost all of the Zn^{2+} ions were chelated by I-HSA. The results imply that the inhibition effect of I-HSA on $\text{A}\beta_{42}$ aggregation increased with an increase in concentration. Furthermore, the inhibition capability of I-HSA on Zn^{2+} -induced aggregation was more prominent than that of HSA and A-HSA at the same concentration due to I-HSA's stronger metal-chelate activity and the greater number of carboxyl groups on the I-HSA surface (Figure 2a, Lanes 8,9,12). As for the case of Cu^{2+} , similar results were observed, as shown in Figure S2a. This confirms that I-HSA had a prominent inhibitory potency on Cu^{2+} -associated $\text{A}\beta_{42}$ aggregation. The ThT assays with the two metal ions proved that I-HSA not only significantly inhibited the self-aggregation of $\text{A}\beta_{42}$ but also effectively alleviated the effect of metal ions on $\text{A}\beta_{42}$ aggregation.

To further explore the effect of I-HSA, we used stopped-flow fluorescence spectroscopy to study the kinetics of Zn^{2+} -mediated $\text{A}\beta_{42}$ aggregation in a time scale of seconds (Figure 2b). It is seen that the light-scattering intensity of $\text{Zn}^{2+}-\text{A}\beta_{42}$ aggregates increased quickly over time and that $\text{A}\beta_{42}$ aggregate size and aggregation rate increased with Zn^{2+} concentration. Additions of IDA, HSA, and I-HSA into the $\text{Zn}^{2+}-\text{A}\beta_{42}$ system decreased the aggregate size and aggregation rate, and the effect of I-HSA was the greatest. When the Zn^{2+} concentration was increased to 160 μM , the signals of the $\text{Zn}^{2+}-\text{A}\beta_{42}$ system with 5 μM I-HSA remained unchanged over time, implying that 5 μM I-HSA could completely inhibit the fast binding of 160 μM Zn^{2+} to $\text{A}\beta_{42}$.

TEM assays indicate that $\text{A}\beta_{42}$ alone exhibited serried and entangled fibrils with a large size distribution (Figure S3a), which is consistent with previous reports.^{3,31} When $\text{A}\beta_{42}$ was incubated with equimolar I-HSA, the aggregates became amorphous and were of shorter lengths (Figure S3b), suggesting that I-HSA altered the pathway of $\text{A}\beta_{42}$ aggregation. As shown in Figure 2c, equimolar Zn^{2+} changed the morphology into spherical aggregates with smaller size distribution, consistent with literature data.^{31,32} In the presence of equimolar I-HSA, the Zn^{2+} -mediated $\text{A}\beta_{42}$ aggregates displayed nonfibrillar morphology (Figure 2d), implying that I-HSA inhibited the formation of $\text{Zn}^{2+}-\text{A}\beta_{42}$ aggregates. Moreover, as shown in Figure S2b,c, I-HSA also disturbed

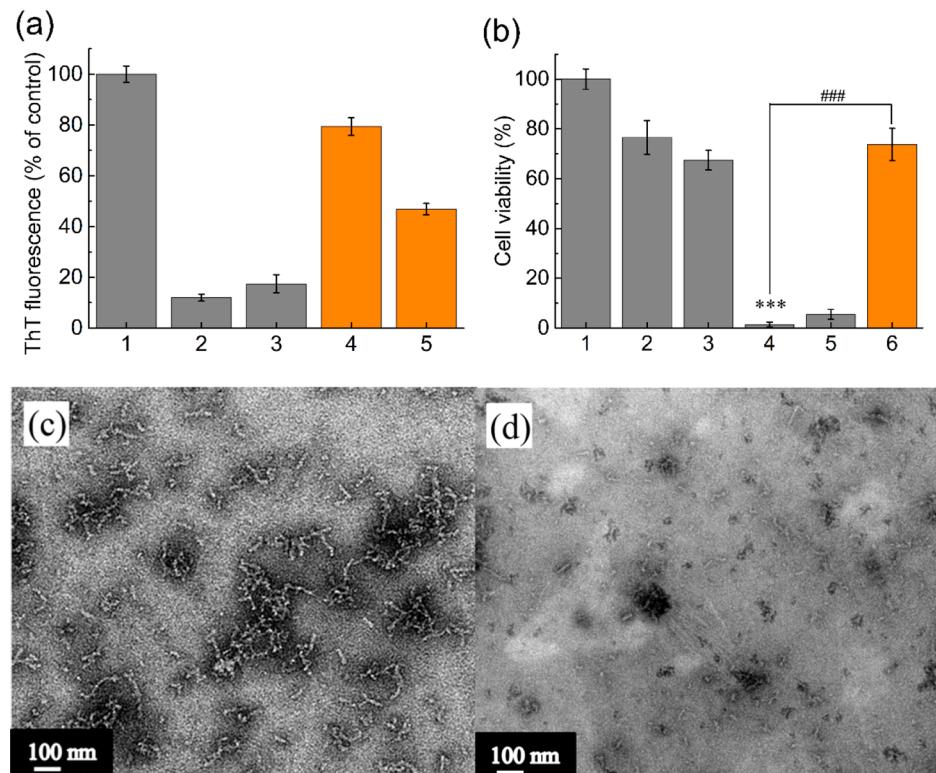


Figure 3. Inhibition of high-concentration ($250 \mu\text{M}$) Zn^{2+} -mediated $\text{A}\beta_{42}$ aggregation and cytotoxicity by I-HSA for 24 h. The final concentrations of $\text{A}\beta_{42}$, HSA, and I-HSA were all $25 \mu\text{M}$ unless stated otherwise. (a) Normalized ThT fluorescence intensities for the inhibition of $\text{A}\beta_{42}$ aggregation. Lanes denote the following conditions: 1, $\text{A}\beta_{42}$ alone; 2, $\text{A}\beta_{42} + \text{Zn}^{2+}$; 3, $\text{A}\beta_{42} + \text{Zn}^{2+} + \text{HSA}$; 4, $\text{A}\beta_{42} + \text{Zn}^{2+} + 12.5 \mu\text{M}$ I-HSA; 5, $\text{A}\beta_{42} + \text{Zn}^{2+} + 25 \mu\text{M}$ I-HSA. (b) Viability of SH-SY5Y cells incubated with Lane 1, buffer A; Lane 2, Zn^{2+} ; Lane 3, $\text{A}\beta_{42}$ fibrils; Lane 4, Zn^{2+} -mediated $\text{A}\beta_{42}$ aggregates; Lane 5, Zn^{2+} -mediated $\text{A}\beta_{42}$ aggregates with HSA; Lane 6, Zn^{2+} -mediated $\text{A}\beta_{42}$ aggregates with I-HSA. ***, $p < 0.001$ as compared to Lane 1. The values of $p < 0.001$ for the pairs of data sets are marked with ***. (c) TEM image of $\text{A}\beta_{42}$ in the presence of Zn^{2+} . (d) TEM image of $\text{A}\beta_{42}$ in the presence of Zn^{2+} and I-HSA.

the Cu^{2+} -mediated $\text{A}\beta_{42}$ aggregation pathway and altered the morphology of Cu^{2+} -mediated $\text{A}\beta_{42}$ aggregates.

The above ThT and TEM analyses revealed that the metal– $\text{A}\beta_{42}$ aggregates with a small β -sheet structure had low ThT intensities (Figure 2a, Lane 6 and Figure S2a, Lane 6), despite the presence of a lot of aggregates as observed by TEM (Figure 2c and Figure S2b). I-HSA effectively directed the metal– $\text{A}\beta_{42}$ aggregation to form unstructured morphologies due to its strong metal-chelate activity and inhibition effect on the self-aggregation of $\text{A}\beta_{42}$ (Figure 2d and Figure S2c). However, the unstructured aggregates contained more β -sheet structures than metal– $\text{A}\beta_{42}$ aggregates, as seen by the higher ThT intensities (Figure 2a and Figure S2a). As a result, the ThT signals of I-HSA-mediated metal– $\text{A}\beta_{42}$ aggregates were higher than those of the metal– $\text{A}\beta_{42}$ aggregates, despite the presence of few fibrils observed by TEM.

Moreover, we carried out sodium dodecyl sulfate–polyacrylamide gel electrophoresis (SDS-PAGE) to analyze the structure changes and size distributions of metal-mediated $\text{A}\beta_{42}$ aggregation by the method described previously.^{3,33} For clearer detection, the analyses were conducted with two gels of different fractionation ranges (Figure S4). In the absence of HSA/I-HSA, only low-MW metal– $\text{A}\beta_{42}$ species ($\text{MW} \leq 10 \text{ kDa}$) were detected (Figure S4a, Lanes 2,6), implying that no SDS-stable $\text{A}\beta_{42}$ aggregates were formed, which was consistent with literature data.³³ However, HSA/I-HSA induced the formation of high MW SDS-stable metal– $\text{A}\beta_{42}$ aggregates ($\text{MW} \geq 50 \text{ kDa}$) (Figure S4b, Lanes 3,4,7,8). This

demonstrates that different types of metal– $\text{A}\beta_{42}$ species formed under the function of HSA/I-HSA. In addition, some oligomers of $\sim 30 \text{ kDa}$ were detected in the presence of HSA, while these aggregates did not appear in the presence of I-HSA (Figure S4b, Lanes 3,4,7,8), indicating that I-HSA displayed an enhanced ability to generate and stabilize high-MW SDS-stable metal– $\text{A}\beta_{42}$ aggregates.

Then, the effects of Zn^{2+} concentration on the ThT fluorescence and cytotoxicity of Zn^{2+} – $\text{A}\beta_{42}$ aggregates were studied (Figure S5). Figure S5a shows that the ThT signals were almost unchanged when Zn^{2+} concentrations exceeded $10 \mu\text{M}$ due to the formation of nonfibrillar aggregates with a small β -sheet structure. However, the cytotoxicity of Zn^{2+} – $\text{A}\beta_{42}$ aggregates remarkably increased with Zn^{2+} concentration (Figure S5b), suggesting that those nonfibrillar aggregates had different cytotoxicity and high-concentration Zn^{2+} -mediated $\text{A}\beta_{42}$ aggregates had higher cytotoxicity. In other words, there was no correlation between ThT and cytotoxicity results, which was consistent with literature data.³⁴ This means that the ThT assay could only provide a quantitative estimation of β -sheet structures contained in $\text{A}\beta_{42}$ aggregates.

The above experimental results have revealed the inhibition effect of I-HSA on the structure and morphology changes of metal-mediated $\text{A}\beta_{42}$ aggregation. Then, we continued to detect the potential protection role of I-HSA on the cytotoxicity of metal– $\text{A}\beta_{42}$ aggregates using 3-(4,5-dimethylthiazol-2-yl)-2,5-diphenyltetrazolium bromide (MTT) and lactate dehydrogenase (LDH) release assays to further confirm the activity of I-

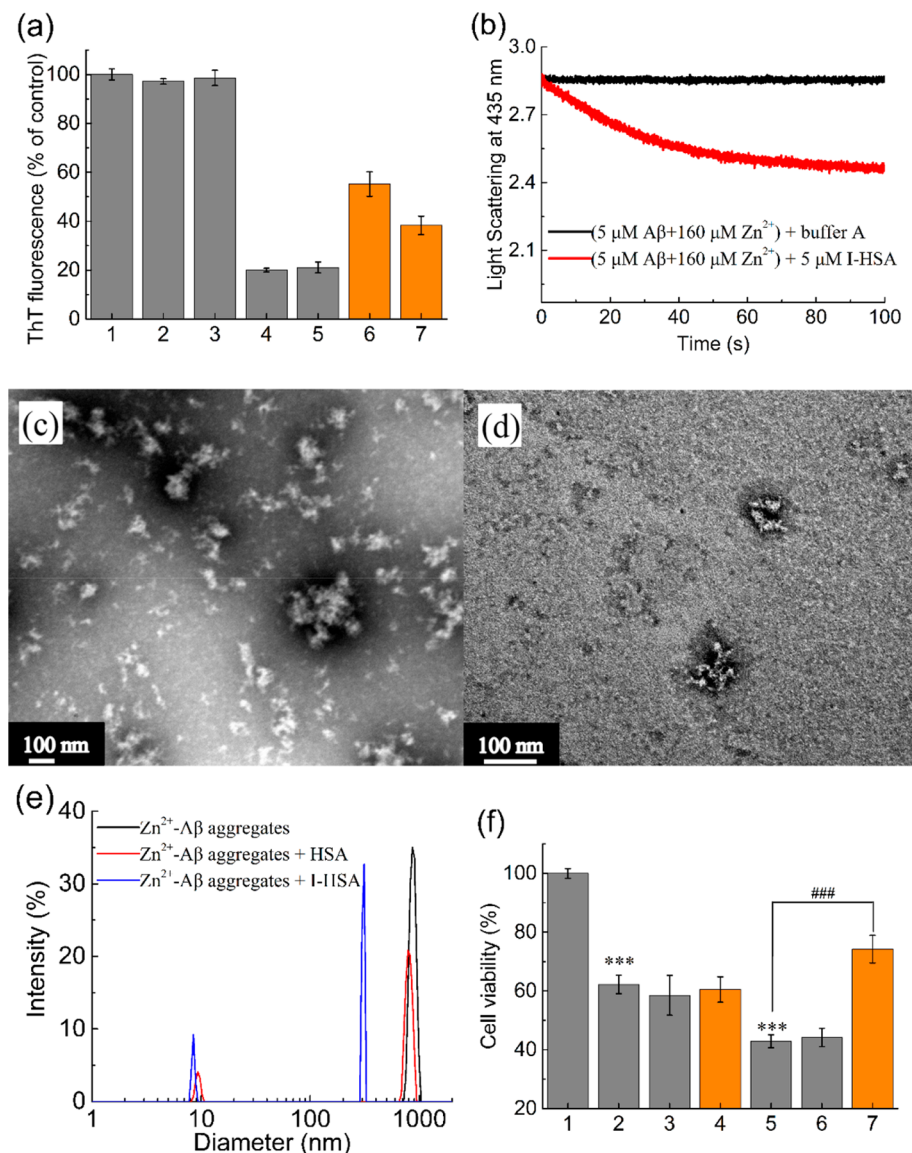


Figure 4. Remodeling effect of I-HSA on mature Zn^{2+} -mediated $A\beta_{42}$ aggregates. (a) Normalized ThT fluorescence intensities for remodeling Zn^{2+} -mediated $A\beta_{42}$ aggregation for 24 h. Lanes denote the following conditions: 1, mature $A\beta_{42}$ fibrils; 2, mature $A\beta_{42}$ aggregates treated with HSA; 3, mature $A\beta_{42}$ aggregates treated with I-HSA; 4, mature Zn^{2+} - $A\beta_{42}$ aggregates; 5, mature Zn^{2+} - $A\beta_{42}$ aggregates treated with HSA; 6, mature Zn^{2+} - $A\beta_{42}$ aggregates treated with 2.5 μM I-HSA; 7, mature Zn^{2+} - $A\beta_{42}$ aggregates treated with 25 μM I-HSA. The final concentrations of $A\beta_{42}$, HSA, and Zn^{2+} were all 25 μM unless stated otherwise. (b) Kinetic traces followed by stopped-flow fluorescence of Zn^{2+} - $A\beta_{42}$ aggregates with or without I-HSA. Samples are as indicated in the legend. (c) TEM image of mature Zn^{2+} - $A\beta_{42}$ aggregates. (d) TEM image of mature Zn^{2+} - $A\beta_{42}$ aggregates after I-HSA treating for 24 h. (e) Size distributions of mature Zn^{2+} - $A\beta$ aggregates without and with HSA/I-HSA treating for 24 h. The final concentrations of $A\beta_{42}$, HSA, I-HSA, and Zn^{2+} were all 25 μM . (f) I-HSA mitigated the cytotoxicity of mature Zn^{2+} - $A\beta_{42}$ aggregates. Lanes denote the following conditions: 1, buffer A; 2, mature $A\beta_{42}$ fibrils; 3, mature $A\beta_{42}$ aggregates treated with HSA; 4, mature $A\beta_{42}$ aggregates treated with I-HSA; 5, mature Zn^{2+} - $A\beta_{42}$ aggregates; 6, mature Zn^{2+} - $A\beta_{42}$ aggregates treated with HSA; 7, mature Zn^{2+} - $A\beta_{42}$ aggregates treated with I-HSA. The final concentrations of $A\beta_{42}$, Zn^{2+} , I-HSA and HSA were all 25 μM . ***, $p < 0.001$ as compared to Lane 1. The values of $p < 0.001$ for the pairs of data sets are marked with ###.

HSA. As shown in Figure 2e (Lane 2), I-HSA presented no cytotoxicity to SH-SY5Y cells, indicating its biocompatibility. By contrast, $A\beta_{42}$ aggregates resulted in the reduction of cell viability to 67.4% (Figure 2e, Lane 4). When equimolar HSA or I-HSA was added, the cell viability increased to 75.4% and 94.1%, respectively, implying that HSA and I-HSA effectively alleviated the cytotoxicity of $A\beta_{42}$ fibrils and that I-HSA had stronger potency than native HSA (Figure 2e, Lanes 5,6). Moreover, as a control, the cell viability changed little with 25 μM Zn^{2+} (Figure 2e, Lane 3), but equimolar Zn^{2+} -mediated $A\beta_{42}$ aggregates showed 48% cytotoxicity (Figure 2e, Lane 7),

which is consistent with literature data.^{3,27} Notably, in the presence of Zn^{2+} -mediated $A\beta_{42}$ aggregates, equimolar I-HSA increased cell viability to 89.1%, distinctly higher than native HSA did (71.9%) (Figure 2e, Lanes 8,9). In the case of Cu^{2+} at pH 6.6, I-HSA also increased the cell viabilities by 44.6% and 110.8% as compared to the $A\beta_{42}$ aggregates- and Cu^{2+} - $A\beta_{42}$ species-treated groups, respectively (Figure S2d). Moreover, by using an alternative cytotoxicity assay method, LDH release assays, similar results were obtained, as shown in Figure S6a,b. The cytotoxicity results with the two metal ions illustrate that I-

HSA could obviously alleviate the cytotoxicity of metal- $\text{A}\beta_{42}$ species much more effectively than HSA.

Finally, to detect the ROS formation by $\text{A}\beta_{42}$ self-aggregation and metal-mediated aggregation, we loaded 2',7'-dichlorofluorescin diacetate (DCFH-DA) into cells by the method described previously.³⁵ I-HSA alone did not alter the ROS level in cells, as shown in Figure 2f (Lane 2). By contrast, $\text{A}\beta_{42}$ fibrils promoted the production of ROS by 20% (Figure 2f, Lane 3), and Cu^{2+} dramatically induced the generation of ROS by a 90% increase (Figure 2f, Lane 5). These data were in agreement with literature data with similar samples.³⁶ However, upon treatment of $\text{A}\beta_{42}$ aggregates and Cu^{2+} - $\text{A}\beta_{42}$ species with equimolar I-HSA, significant decreases in the ROS level were observed (Figure 2f, Lanes 4,6), indicating that equimolar I-HSA suppressed the ROS production mediated by $\text{A}\beta_{42}$ or Cu^{2+} - $\text{A}\beta_{42}$ aggregates. Hence, I-HSA could attenuate the ROS level of $\text{A}\beta_{42}$ and Cu^{2+} - $\text{A}\beta_{42}$ species and avoid the ROS damage on cells.

Overall, the above assays demonstrated that I-HSA significantly mitigated metal-mediated $\text{A}\beta_{42}$ aggregation, the intracellular ROS level, and cytotoxicity. In previous examples from the literature, equimolar selenoprotein P and cyclam derivative increased the cell viability only by 11% and 27%, respectively, as compared to the Cu^{2+} - $\text{A}\beta$ aggregate-treated group.^{19,36} In comparison with the literature results, it is obvious that I-HSA displayed a stronger potency for capturing more metal ions at the same concentration.

I-HSA Inhibits High-Concentration Zn^{2+} -Mediated $\text{A}\beta_{42}$ Aggregation. Aiming at the high-concentration Zn^{2+} in amyloid plaque,⁹ we further detected the effect of 250 μM Zn^{2+} on $\text{A}\beta_{42}$ aggregation and the inhibition potency of I-HSA. As shown in Figure 3a (Lane 2), 250 μM Zn^{2+} almost eliminated the ThT intensities of $\text{A}\beta_{42}$. In this system, native HSA (25 μM) had a negligible effect on the Zn^{2+} -mediated $\text{A}\beta_{42}$ aggregation due to the high Zn^{2+} concentration and the limited metal-chelate capacity of native HSA (Figure 3a, Lane 3). By contrast, 12.5 μM I-HSA could increase the ThT fluorescent signal to 79.4% (Figure 3a, Lane 4), implying that 12.5 μM I-HSA dramatically suppressed the effect of high-concentration Zn^{2+} on $\text{A}\beta_{42}$ aggregation. When I-HSA concentration was increased to 25 μM , the ThT fluorescence intensity reduced to 46.9% of the control group (Figure 3a, Lane 5). The results indicate that 25 μM I-HSA not only chelated the high-concentration Zn^{2+} ions but also effectively inhibited $\text{A}\beta_{42}$ aggregation.

Figure 3b shows that 250 μM Zn^{2+} alone caused about 20% cell death in the MTT assay (Lane 2), and 25 μM $\text{A}\beta_{42}$ caused 33% cell death (Lane 3). However, little cell viability was left with the 250 μM Zn^{2+} -mediated $\text{A}\beta_{42}$ species (Figure 3b, Lane 4). To this high cytotoxicity, native HSA had an inappreciable effect (Figure 3b, Lane 5), but 25 μM I-HSA could keep the cell viability as high as 70% (Figure 3b, Lane 6). LDH release assays also revealed that I-HSA remarkably decreased the LDH release level of high-concentration Zn^{2+} -mediated $\text{A}\beta_{42}$ aggregates (Figure S6c). This proves that I-HSA was highly effective in rescuing cells from the high cytotoxicity caused by high-concentration Zn^{2+} -mediated $\text{A}\beta_{42}$ aggregates.

To get more insight into the effect of I-HSA on high-concentration Zn^{2+} -induced $\text{A}\beta_{42}$ aggregation, TEM observations were performed. In the presence of 250 μM Zn^{2+} , Zn^{2+} - $\text{A}\beta_{42}$ formed amorphous and entangled aggregates (Figure 3c), which were obviously different from those induced by 25 μM Zn^{2+} (Figure 2c). However, the presence of 25 μM I-HSA

altered the entangled Zn^{2+} - $\text{A}\beta_{42}$ aggregates into short rods and small nonfibrillar structures (Figure 3d), which were similar to the aggregates in Figure 2d. This illustrates that 25 μM I-HSA almost completely suppressed the effect of 250 μM Zn^{2+} as did with 25 μM Zn^{2+} on $\text{A}\beta_{42}$ aggregation and cytotoxicity (see Figures 2e and 3b). Namely, I-HSA showed a potent inhibition effect on high-concentration Zn^{2+} -mediated $\text{A}\beta_{42}$ aggregation and cytotoxicity because of its high metal-chelate capacity. Therefore, the dosage of I-HSA can be greatly reduced in the treatment as compared to other chelators.^{3,19,27,36}

I-HSA Remodels Mature Metal-Mediated $\text{A}\beta_{42}$ Aggregates. The remodeling of mature amyloid fibrils is another therapeutic strategy in the treatment of AD.³⁷ Therefore, the capability of eliminating mature metal-mediated $\text{A}\beta_{42}$ aggregates is an important merit of a potential inhibitor. The remodeling effect of I-HSA on mature metal-mediated $\text{A}\beta_{42}$ aggregates was first investigated by ThT assays. As shown in Figure 4a, HSA and I-HSA had no remodeling effect on mature $\text{A}\beta_{42}$ fibrils (Lanes 1–3), and HSA had no effect on Zn^{2+} - $\text{A}\beta_{42}$ aggregates either (Lanes 4,5). By contrast, the addition of 2.5 μM I-HSA into Zn^{2+} - $\text{A}\beta_{42}$ aggregates increased the ThT fluorescent signal from 19.9% to 55.2% due to its metal-chelate capability (Figure 4a, Lane 6). When the I-HSA concentration was increased to 25 μM , the ThT fluorescence intensity reduced to 38.3% of the control (Figure 4a, Lane 7), indicating that I-HSA remodeled Zn^{2+} - $\text{A}\beta_{42}$ aggregates further to form aggregates of less cross- β structures after Zn^{2+} was sequestered. This is evidence that the metal-chelate capability of I-HSA contributed to the prominent remodeling effect on mature Zn^{2+} - $\text{A}\beta_{42}$ aggregates. Similar results were obtained in the system with Cu^{2+} (Figure S7a).

Stopped-flow fluorescence assays were conducted to investigate the effect of I-HSA on Zn^{2+} - $\text{A}\beta_{42}$ aggregation kinetics on a time scale of seconds. As shown in Figure 4b, a pronounced decrease of the scattering signal of the Zn^{2+} - $\text{A}\beta_{42}$ aggregates was detected in the presence of I-HSA, implying that the structure of Zn^{2+} - $\text{A}\beta_{42}$ aggregates changed over time. The results indicate that I-HSA captured Zn^{2+} rapidly and effectively remodeled the Zn^{2+} - $\text{A}\beta_{42}$ species on a time scale of seconds.

Furthermore, TEM was used to analyze the morphology changes of $\text{A}\beta_{42}$ species. As shown in Figure 4c, mature Zn^{2+} - $\text{A}\beta_{42}$ aggregates displayed nonfibrillar structures, consistent with the above ThT assay and literature data.³² However, the aggregates converted into amorphous structures of smaller sizes after being treated with equimolar I-HSA (Figure 4d).

The size distributions of $\text{A}\beta_{42}$ aggregates were then analyzed by dynamic light-scattering (DLS) measurements. Although $\text{A}\beta_{42}$ fibrils are heterogeneous and nonspherical by nature, the calculated hydrodynamic diameter by DLS can reflect the changes in $\text{A}\beta$ conformation and provide a qualitative estimation of their size distributions.^{27,28,31} Therefore, we used DLS to analyze the size-distribution changes of I-HSA and the amyloid aggregates at different conditions. Figure S8 shows that the size distribution of I-HSA remained stable after interaction with Zn^{2+} or $\text{A}\beta_{42}$, as evidenced by the inappreciable changes of the molecular size ($\sim 10 \text{ nm}$). However, the sizes of mature Zn^{2+} - $\text{A}\beta_{42}$ aggregates decreased after being treated with equimolar I-HSA (Figure 4e), consistent with the TEM results in Figure 4c,d. By contrast, native HSA did not influence the size of mature Zn^{2+} - $\text{A}\beta_{42}$ aggregates (Figure 4e), indicating that HSA had no remodeling effect. The results further confirmed that I-HSA had a remodeling effect that altered the morphology and structure of mature metal- $\text{A}\beta_{42}$ aggregates.

Cell-viability assays were conducted to reveal the biological implication of the remodeling effect of I-HSA. It is seen that the effects of HSA and I-HSA on the cytotoxicity of mature $A\beta_{42}$ fibrils were negligible (Figure 4f, Lanes 3,4), which is in good agreement with the ThT data (Figure 4a, Lanes 2,3). Mature $Zn^{2+}-A\beta_{42}$ aggregates reduced the cell viability to 42.9%, and native HSA had no effect on the cytotoxicity of mature $Zn^{2+}-A\beta_{42}$ species (Figure 4f, Lanes 5,6). In contrast, coincubation of $Zn^{2+}-A\beta_{42}$ aggregates and equimolar I-HSA pronouncedly increased the cell viability to 74.2% (Figure 4f, Lane 7), indicating that the remodeling effect of I-HSA on mature $Zn^{2+}-A\beta_{42}$ species was very effective in protecting the cells. Similar results were obtained in the system with Cu^{2+} (Figure S7b), in which I-HSA increased the cell viability from 35.2% to 74.6%. In addition, as shown in Figure S6d,e, I-HSA decreased the LDH release level by mature metal- $A\beta_{42}$ aggregates, suggesting that I-HSA effectively mitigated the cytotoxicity of mature metal- $A\beta_{42}$ aggregates.

Fischer et al. reported that the thiophosphate of adenosine diphosphate ($ADP-\beta-S$) was able to remodel preformed metal- $A\beta_{42}$ aggregates efficiently, but the addition of 3 equiv of $ADP-\beta-S$ to mature $Zn^{2+}-A\beta_{42}$ aggregates only disaggregated about 36% of the species.³⁸ Moreover, 5 equiv of histidine was found to inhibit the formation of $Cu^{2+}-A\beta$ aggregates but did not affect mature $Cu^{2+}-A\beta$ aggregates.³⁹ Therefore, I-HSA shows a remarkable advantage over previously reported inhibitors, as equimolar I-HSA increased the cell viability by 112% compared to the $Cu^{2+}-A\beta_{42}$ aggregate-treated group.

Mechanistic Discussion. By summarizing the above results obtained from biophysical and biological analyses, we proposed a mechanistic model to interpret the multifunctional effects of I-HSA on metal-mediated $A\beta_{42}$ aggregation and cytotoxicity (Figure 5). In the on-pathway aggregation, $A\beta_{42}$ monomers self-assemble into oligomers and amyloid fibrils of high cytotoxicity (Figure 2e, Lane 4).⁵ Metal ions facilitate the formation of amorphous metal- $A\beta_{42}$ aggregates rather than amyloid fibrils with β -sheet structures (Figure 5a). The very high cytotoxicity of metal- $A\beta_{42}$ species definitely comes from the neurotoxic aggregates themselves and the production of ROS in cells (Figure 2e,f).¹³ However, I-HSA alters the pathway of metal-associated $A\beta_{42}$ aggregation by chelating a majority of metal ions and alleviates the cytotoxicity of metal- $A\beta_{42}$ species and the ROS damage on nerve cells very effectively (Figure 5b). Due to its high metal-chelate capacity, I-HSA can effectively mitigate high-concentration metal-mediated $A\beta_{42}$ aggregation and cytotoxicity (Figure 3). Besides, I-HSA remodels mature metal- $A\beta_{42}$ species into amorphous aggregates of less cytotoxicity (Figure 5c). As shown in Figure 4a, the high metal-chelate capability of I-HSA contributed to the prominent remodeling effect. After the metal ions were sequestered, the structure of $A\beta_{42}$ aggregates became unstable, leading to the size and morphology changes (Figure 4d,e). It is the reason that I-HSA effectively remodeled metal-associated $A\beta_{42}$ aggregates but showed an inappreciable effect on mature $A\beta_{42}$ fibrils (Figure 4).

On the A-HSA effect on inhibiting $A\beta$ self-aggregation and metal-mediated aggregation, we previously proposed a hydrophobic binding-electrostatic repulsion (HyBER) mechanism.^{27,28} The HyBER mechanism should also work on the prominent effects of I-HSA, which also has extra negative charges introduced by IDA coupling on the protein surface. In brief (Figure 5d), $A\beta_{42}$ is bound to I-HSA surface through hydrophobic interactions. Meanwhile, the bound $A\beta_{42}$ receives

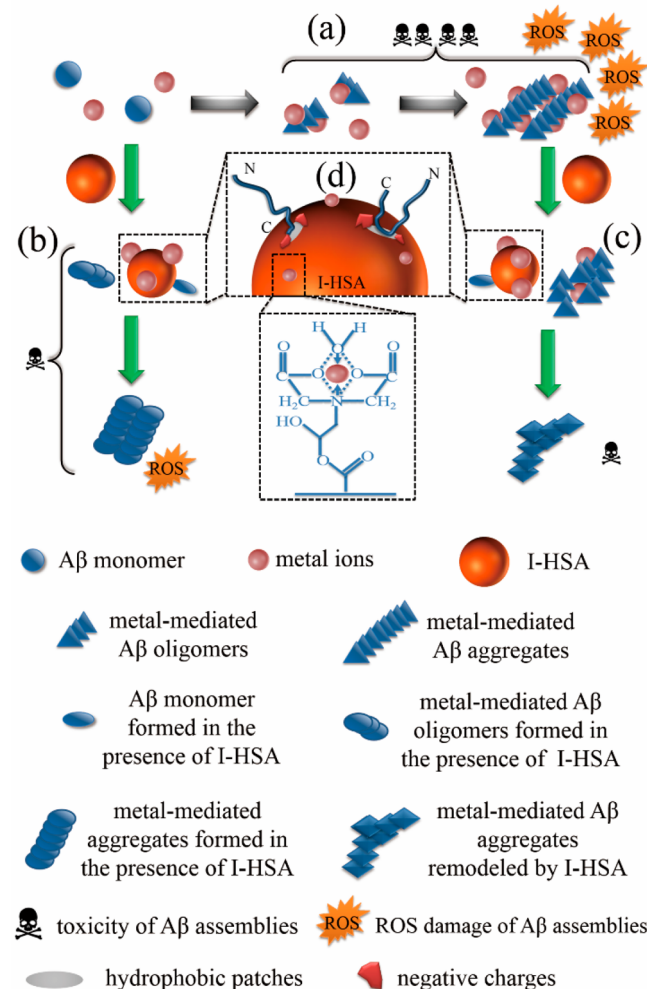


Figure 5. Schematic representation of the multifunctional effects of I-HSA on metal-mediated $A\beta_{42}$ aggregation and cytotoxicity. (a) Metal-mediated $A\beta_{42}$ aggregation: metal ions induce formation of metal- $A\beta_{42}$ aggregates of even higher neurotoxicity and ROS level. (b) Metal-mediated $A\beta_{42}$ aggregation in the presence of I-HSA: I-HSA binds metal ions and inhibits metal- $A\beta_{42}$ aggregation, cytotoxicity and ROS damage. (c) Remodeling effect of I-HSA on metal-mediated $A\beta_{42}$ aggregates: I-HSA remodels mature metal-mediated $A\beta_{42}$ aggregates into less toxic structure. (d) A schematic representation of the HyBER mechanism and the metal-chelating way on I-HSA surface.

electrostatic repulsion from the anionic surface of I-HSA. The two opposite forces give rise to the extension of $A\beta_{42}$ conformation, which alters the pathway of $A\beta_{42}$ self-aggregation and metal-mediated aggregation into unstructured aggregates of low cytotoxicity and ROS damage. Taken together, I-HSA works as a potent multifunctional agent in inhibiting and remodeling metal-induced $A\beta_{42}$ aggregation, cytotoxicity, and ROS damage.

Finally, the blood-brain barrier (BBB) penetrations of HSA and I-HSA were evaluated by using a parallel artificial membrane permeation assay (PAMPA).^{40,41} According to the literature data, samples with permeability (P_e) values greater than $4.7 \times 10^{-6} \text{ cm/s}$ are regarded as being capable of crossing the BBB effectively, while those with $P_e < 1.8 \times 10^{-6} \text{ cm/s}$ possess low BBB permeation by passive diffusion.^{40,41} As listed in Table S2, the P_e values of HSA and I-HSA were 1.52×10^{-6} and $1.43 \times 10^{-6} \text{ cm/s}$, respectively, indicating that both of

them exhibited low BBB permeation. This is a critical problem to be solved in further development of I-HSA as a multifunctional agent against metal-induced amyloid cytotoxicity. Fortunately, proteins like HSA can be easily modified and, there are previously reported methods in the literature for improving the permeation of macromolecules and nanoparticles to cross the BBB.^{42,43} For example, Chang et al. used a monoclonal antibody against mouse transferrin receptor to ferry tumor necrosis factor alpha inhibitors across the BBB effectively.⁴² In addition, the conjugates of nanoparticles and short peptide (glycoheptapeptides) were confirmed to cross the BBB successfully by endocytosis.⁴³ Hence, further research on I-HSA should direct toward the conjugation of a cell-penetration peptide to improve its BBB permeation.

CONCLUSIONS

In this study, we have developed I-HSA as a multifunctional agent for inhibiting and remodeling metal-mediated $\text{A}\beta_{42}$ aggregation, cytotoxicity, and ROS damage on nerve cells. I-HSA maintains the stability and biocompatibility as native HSA does. The modification not only enhanced the chelating capability but also increased the negative charges on HSA surface. As a result, I-HSA shows more prominent inhibitory potency on metal-mediated $\text{A}\beta_{42}$ aggregation and cytotoxicity than the agents reported in literature. Noticeably, I-HSA can alleviate the influence of high-concentration Zn^{2+} on $\text{A}\beta_{42}$ aggregation, so the dosage of I-HSA can be greatly reduced as compared to other chelators. Also, I-HSA remarkably attenuates the ROS damage caused by $\text{A}\beta_{42}$ and Cu^{2+} - $\text{A}\beta_{42}$ species on nerve cells. Finally, I-HSA remodels mature metal- $\text{A}\beta_{42}$ species into unstructured aggregates of low cytotoxicity. The results demonstrate that the extra negative charges introduced by coupling IDA on the I-HSA surface are beneficial in the inhibition of metal-mediated $\text{A}\beta_{42}$ aggregation. Taken together, our results show that I-HSA is a potent multifunctional agent for inhibiting and remodeling metal-induced $\text{A}\beta_{42}$ aggregation, cytotoxicity, and ROS damages. To our knowledge, I-HSA is the first multifunctional macromolecule for inhibiting high-concentration metal-induced $\text{A}\beta$ aggregation and remodeling mature metal-induced $\text{A}\beta$ species. The findings provided new insights into the design of potent agents against metal-mediated $\text{A}\beta$ aggregation.

METHODS

Materials. $\text{A}\beta_{42}$ from GL Biochem (Shanghai, China) was synthesized using routine solid-phase peptide synthesis and Fmoc chemistry. HSA, IDA, zinc chloride, copper chloride, DCFH-DA, dimethyl sulfoxide (DMSO), phosphotungstic acid, HEPES, sodium borate, MTT, ThT, 1,1,1,3,3-hexafluoro-2-propanol (HFIP), boric acid, 1,4-butanediol diglycidyl ether, glycerol, bromophenol blue, sodium dodecyl sulfate (SDS), polyacrylamide, silver nitrate, methanol, acetic acid, sodium thiosulfate, sodium carbonate, and formaldehyde were received from Sigma (St. Louis, MO, U.S.A.). The LDH assay kit was purchased from Roche (Mannheim, Germany). Porcine brain lipid (PBL) was obtained from Avanti Polar Lipids (Alabaster, AL, U.S.A.). Sephadex G25 gel was purchased from GE Healthcare (Uppsala, Sweden). Human neuroblastoma SH-SY5Y cells were obtained from the Cell Bank of the Chinese Academy of Sciences (Shanghai, China). Fetal bovine serum (FBS) and Dulbecco's Modified Eagle's Medium/Ham's Nutrient Mixture F-12 (DMEM/F12) were purchased from Invitrogen (Carlsbad, CA, U.S.A.). All other chemicals were of the highest purity available from local sources.

Synthesis and Characterization of I-HSA. The synthesis of I-HSA is illustrated in Figure 1. At first, HSA powder was dissolved in borate buffer (0.2 M, pH 9.0) at 10 mg/mL, and then 1,4-butanediol

diglycidyl ether (110 μL) was slowly added to the protein solution. After the reaction at 120 rpm and 37 °C in a shaking water bath for 12 h, the reaction mixture was loaded onto Sephadex G25 column (16 mm I.D., 20 cm in length) to recover the modified HSA by size-exclusion chromatography on an AKTA Explorer 100 system (GE Healthcare, Uppsala, Sweden). The column was washed with the borate buffer at 1 mL/min, and the epoxy-activated intermediate product (Figure 1a) was collected. Then, IDA powder (500 mg) was dissolved into the intermediate product solution, the reaction (Figure 1b) continued at 37 °C for 24 h, and the reaction mixture was loaded onto the above column to recover I-HSA. The purified I-HSA was freeze-dried and stored at -20 °C before use.

As described previously,²⁷ the MWs of HSA, the intermediate product, and I-HSA in deionized water at 1 mg/mL were measured by matrix-assisted laser desorption ionization time-of-flight mass spectroscopy (Autoflex Tof/TofIII, Bruker Daltonics, MA, U.S.A.) to determine the modification degree of I-HSA. The sizes and zeta potentials of HSA and I-HSA (25 μM each) were determined by Zetasizer Nano (Malvern Instruments, Worcestershire, U.K.) in buffer A at 25 °C. A circular dichroism spectrometer (JASCO J-815, Tokyo, Japan) and fluorescence spectrometer (Perking Elmer LS-55, MA, U.S.A.) were respectively used to analyze the secondary and tertiary structures of the proteins at 25 μM in buffer A at 25 °C.

$\text{A}\beta_{42}$ Sample Preparation and Incubation. $\text{A}\beta_{42}$ monomer was pretreated with HFIP to eliminate pre-existing $\text{A}\beta_{42}$ aggregates by a reported method.⁴⁴ Immediately prior to use, the treated $\text{A}\beta_{42}$ was dissolved in 20 mM NaOH and sonicated for 20 min.²⁷ To ensure the binding of metal ions to $\text{A}\beta_{42}$, Zn^{2+} in buffer A or Cu^{2+} in buffer B was added into the $\text{A}\beta_{42}$ monomer solution. Then 2 min later, HSA/I-HSA was added into the metal- $\text{A}\beta_{42}$ sample and mixed uniformly. The final concentration of $\text{A}\beta_{42}$ was 25 μM , and the samples were incubated at 37 °C with continuous shaking at 150 rpm for 24 h.

For remodeling assays on mature metal- $\text{A}\beta_{42}$ aggregates, $\text{A}\beta_{42}$ samples were prepared, as described above. After 24 h of incubation, different concentrations of HSA/I-HSA solution were added to the mature $\text{A}\beta_{42}$ samples. The final concentration of $\text{A}\beta_{42}$ was 25 μM , and the samples were incubated at 37 °C with continuous shaking at 150 rpm for 24 h.

Thioflavin T Fluorescence Assay. The ThT fluorescence assay was used to quantitatively assess $\text{A}\beta_{42}$ aggregation.⁴⁵ In the assay, an incubated $\text{A}\beta_{42}$ sample (200 μL) was added into 2 mL of ThT buffer (25 μM ThT in 20 mM HEPES, pH 6.0) and mixed uniformly, as described previously.²⁷ The ThT fluorescence intensity was measured with excitation and emission at 440 and 480 nm, respectively, by a fluorescence spectrometer (Perking Elmer LS-55, MA, U.S.A.) at 25 °C.

Transmission Electron Microscopy. TEM assays were used to monitor the morphologies of $\text{A}\beta_{42}$ aggregates. An $\text{A}\beta_{42}$ sample was dropped onto a carbon-coated copper grid (300 mesh) and dried in the air for 5 min. Then, the grid was negatively stained with 2% (w/v) of phosphotungstic acid (10 μL) for another 5 min.²⁷ Observation was performed on a JEM-2100F TEM (JEOL Inc., Tokyo, Japan) with an accelerating voltage of 200 kV.

Dynamic Light-Scattering Measurements. The size distribution of $\text{A}\beta_{42}$ samples were analyzed using Nanosizer (Malvern Instruments, Worcestershire, UK) at 25 °C.²⁷ In the analysis, 1.2 mL of $\text{A}\beta_{42}$ sample was transferred into a disposable cuvette and measured at 25 °C.

Cell-Viability Assay. To detect the cytotoxicity of $\text{A}\beta_{42}$ species, MTT assays were employed. The human neuroblastoma SH-SY5Y cells were cultured in DMEM/F12 medium with 20% FBS at 37 °C under 5% CO₂. The cells were seeded for 24 h in a 96-well plate at a density of 5×10^3 cells per well. Then, preincubated $\text{A}\beta_{42}$ samples (25 μM) were introduced to the cells for additional 24 h at 37 °C in a CO₂ cell-culture box (NAPCO 5410, Tualatin, Oregon, U.S.A.). The final concentration of $\text{A}\beta_{42}$ in the cells was 5 μM . Afterward, a volume of 10 μL of MTT solution (6 mg/mL in buffer A) was added into each well and incubated for another 4 h. Lastly, the medium was discarded and the cells were fully lysed with DMSO. The absorbance at 570 nm was

determined by a multimode microplate reader (TECAN Austria GmbH, Salzburg, Austria) to assess the cytotoxicity of $\text{A}\beta_{42}$ species.

LDH release assays were also conducted for the quantification of cell death, as described previously.⁴⁶ In this work, the end-point $\text{A}\beta_{42}$ products after 24 h of seeding were added into the cell-culture media and incubated for 48 h. The cultured cells were centrifuged at 400g for 5 min, and then 80 μL of the supernatant was collected and mixed with 40 μL of the reaction buffer. After the supernatant and reaction buffer were mixed for 30 min, the LDH release level was assessed at a test wavelength of 490 nm and a reference wavelength of 630 nm. As a control, the cells were incubated with 1% (v/v) Triton X-100 to get a representative maximal LDH release as 100% cytotoxicity.

Measurement of Intracellular Reactive Oxygen Species. The effects of $\text{A}\beta_{42}$ species on ROS formation in cells were performed with the fluorescent probe DCFH-DA, as described previously.^{47,48} SH-SY5Y cells were cultured with $\text{A}\beta_{42}$ samples for 24 h at 37 °C, as described above. Then, the cells were washed twice with buffer A and incubated with 10 μM DCFH-DA in FBS-free medium at 37 °C in the CO₂ cell-culture box. After 30 min of incubation, the cells were washed twice with FBS-free medium to remove excess DCFH-DA. Finally, the intracellular ROS level was examined with excitation and emission at 488 and 535 nm, respectively, by the multimode microplate reader mentioned above.

Stopped-Flow Fluorescence Measurements. The Rayleigh light-scattering intensity over time was detected with excitation at 435 nm to study $\text{A}\beta$ aggregation states on a time scale of seconds.⁴⁹ We employed SX 20 stopped-flow fluorescence instrument (Applied Photophysics, Leatherhead, U.K.) to measure the binding kinetics of $\text{A}\beta_{42}$ and Zn²⁺ in buffer A in the presence or absence of HSA/I-HSA/IDA on a time scale of seconds at 37 °C, as we described previously.^{27,46} The final $\text{A}\beta_{42}$ and HSA/I-HSA/IDA concentrations were all 5 μM .

SDS-PAGE. $\text{A}\beta_{42}$ samples obtained by incubation for 24 h were diluted with a loading buffer (100 mM Tris buffer at pH 6.8, 20% (v/v) glycerol, 0.2% bromophenol blue, and 4% SDS) to create working solutions, as described previously.⁵⁰ The samples were not preheated. A 10 μL aliquot of each working solution was run on a 16% or 12% polyacrylamide gel with a 4% stacking polyacrylamide gel. The gels were run at a constant voltage (100 V). After an electrophoretic operation, the gel was successively treated by shaking in a fixing solution (50% (v/v) methanol and 5% (v/v) acetic acid), 50% (v/v) aqueous methanol, and deionized water. Then the gel was sensitized with 0.02% (w/v) sodium thiosulfate and was rinsed with deionized water twice. After the last rinse, the gel was submerged in chilled 0.1% (w/v) silver nitrate in deionized water and shaken at 4 °C for 20 min. Next, the gel was rinsed with deionized water twice again. To develop the gel, the gel was incubated in a developing solution (2% (w/v) sodium carbonate and 0.04% (w/v) formaldehyde) until the desired intensity of staining was reached. The development was stopped by discarding the developing solution and submerging the gel in 5% acetic acid solution.

PAMPA-BBB assays. The PAMPA was performed to evaluate the BBB penetration properties of HSA and I-HSA as described previously.^{40,41} In brief, HSA and I-HSA were dissolved in a solution of 70% PB (50 mM sodium phosphate, pH 7.4) and 30% ethanol (v/v) to a concentration of 3.5 mg/mL, in the presence of 2% (v/v) DMSO. In the experiment, the donor microplate (Millipore, Billerica, MA, U.S.A.) was impregnated with 4 μL of PBL (20 mg/mL in dodecane) and filled with 200 μL of sample. Meanwhile, 300 μL of PB/ethanol (7:3) was added to the acceptor microplate (Millipore, Billerica, MA, U.S.A.). Then, the donor microplate was carefully placed on the acceptor microplate, and left undisturbed for 10 h at 25 °C. After that, a 96-well plate was used to determine the concentration of samples in the acceptor wells. The permeability of HSA/I-HSA was calculated using the following equation:

$$P_e = - \left(\frac{V_d V_a}{(V_d + V_a) At} \right) \ln \left(1 - \frac{[\text{drug}]_{\text{acceptor}}}{[\text{drug}]_{\text{equilibrium}}} \right)$$

where V_d is the volume in the donor well, V_a is the volume in the acceptor well, A is the filter area, t is the permeation time, $[\text{drug}]_{\text{acceptor}}$ is the absorbance of the compound in the acceptor well, and $[\text{drug}]_{\text{equilibrium}}$ is the theoretical equilibrium absorbance.

Statistical Analysis. In the above experiments, each measurement was repeated at least three times, and the mean value and standard errors were calculated. Statistical comparisons were conducted using one-way analysis of variance followed by Student's *t* test, and $p < 0.05$ or less was considered to be statistically significant.

ASSOCIATED CONTENT

S Supporting Information

The Supporting Information is available free of charge on the ACS Publications website at DOI: [10.1021/acscchemneuro.7b00128](https://doi.org/10.1021/acscchemneuro.7b00128).

Characterization of the physicochemical properties of HSA and I-HSA, the permeability of HSA and I-HSA in the PAMPA, fluorescence spectra and circular dichroism spectra of HSA and I-HSA, inhibition of Cu²⁺-mediated $\text{A}\beta_{42}$ aggregation and cytotoxicity by I-HSA, TEM images of $\text{A}\beta_{42}$ aggregates, analysis of the size distributions of metal- $\text{A}\beta_{42}$ aggregates by SDS-PAGE, influence of Zn²⁺ concentration on $\text{A}\beta_{42}$ aggregation and cytotoxicity, inhibitory effect of I-HSA on the cytotoxicity of $\text{A}\beta_{42}$ aggregates by LDH assays, remodeling effect of I-HSA on mature Cu²⁺-mediated $\text{A}\beta_{42}$ aggregates and size distributions of I-HSA without and with Zn²⁺ or $\text{A}\beta_{42}$ aggregates (PDF)

AUTHOR INFORMATION

Corresponding Author

*Tel: +86 22 27403389; Fax: +86 22 27403389; E-mail: ysun@tju.edu.cn

ORCID

Xiaoyan Dong: [0000-0002-8040-5897](https://orcid.org/0000-0002-8040-5897)

Yan Sun: [0000-0001-5256-9571](https://orcid.org/0000-0001-5256-9571)

Author Contributions

B.X., H.Z., and X.L. contributed equally to this work. Y.S. designed the research; B.X., H.Z., X.L., and X.D. performed the experiments and analyzed the data. B.X., H.Z., X.L., X.D., and Y.S. wrote or contributed to the writing of the manuscript.

Funding

This work was funded by the National Natural Science Foundation of China (Nos. 21376172, 91634119, 21561162005, and 21621004) and the Natural Science Foundation of Tianjin from Tianjin Municipal Science and Technology Commission (Contract No. 16JCZDJC32300).

Notes

The authors declare no competing financial interest.

REFERENCES

- Huang, Y., and Mucke, L. (2012) Alzheimer mechanisms and therapeutic strategies. *Cell* **148**, 1204–1222.
- Thapa, A., Jett, S. D., and Chi, E. Y. (2016) Curcumin Attenuates Amyloid- β Aggregate Toxicity and Modulates Amyloid- β Aggregation Pathway. *ACS Chem. Neurosci.* **7**, 56–68.
- Hyung, S. J., DeToma, A. S., Brender, J. R., Lee, S., Vivekanandan, S., Kochi, A., Choi, J. S., Ramamoorthy, A., Ruotolo, B. T., and Lim, M. H. (2013) Insights into antiamyloidogenic properties of the green tea extract (−)-epigallocatechin-3-gallate toward metal-associated amyloid-beta species. *Proc. Natl. Acad. Sci. U. S. A.* **110**, 3743–3748.
- Turner, J. P., Lutz-Rechtein, T., Moore, K. A., Rogers, L., Bhave, O., Moss, M. A., and Servoss, S. L. (2014) Rationally designed

- peptides modulate aggregation of amyloid-Beta 40. *ACS Chem. Neurosci.* 5, 552–558.
- (5) Wang, Q., Yu, X., Patal, K., Hu, R., Chuang, S., Zhang, G., and Zheng, J. (2013) Tanshinones Inhibit Amyloid Aggregation by Amyloid- β Peptide, Disaggregate Amyloid Fibrils, and Protect Cultured Cells. *ACS Chem. Neurosci.* 4, 1004–1015.
- (6) Rajasekhar, K., Madhu, C., and Govindaraju, T. (2016) A natural tripeptide-based inhibitor of multifaceted amyloid β toxicity. *ACS Chem. Neurosci.* 7, 1300–1310.
- (7) Rajasekhar, K., Chakrabarti, M., and Govindaraju, T. (2015) Function and toxicity of amyloid beta and recent therapeutic interventions targeting amyloid beta in alzheimer's disease. *Chem. Commun.* 51, 13434–13450.
- (8) James, S. A., Churches, Q. I., de Jonge, M. D., Birchall, I. E., Streltsov, V., McColl, G., Adlard, P. A., and Hare, D. J. (2017) Iron, Copper, and Zinc Concentration in $A\beta$ Plaques in the APP/PS1Mouse Model of Alzheimer's Disease Correlates with Metal Levels in the Surrounding Neuropil. *ACS Chem. Neurosci.* 8, 629–637.
- (9) Guzzi, R., Rizzuti, B., Labate, C., Zappone, B., and De Santo, M. P. (2015) Ferric Ions Inhibit the Amyloid Fibrillation of beta-Lactoglobulin at High Temperature. *Biomacromolecules* 16, 1794–1801.
- (10) Huy, P. D. Q., Vuong, Q. V., La Penna, G., Faller, P., and Li, M. S. (2016) Impact of Cu(II) Binding on Structures and Dynamics of $A\beta$ 42 Monomer and Dimer: Molecular Dynamics Study. *ACS Chem. Neurosci.* 7, 1348–1363.
- (11) Barnham, K. J., and Bush, A. I. (2014) Biological metals and metal-targeting compounds in major neurodegenerative diseases. *Chem. Soc. Rev.* 43, 6727–6749.
- (12) Jiang, D., Zhang, L., Grant, G. P. G., Dudzik, C. G., Chen, S., Patel, S., Hao, Y., Millhauser, G. L., and Zhou, F. (2013) The elevated copper binding strength of amyloid- β aggregates allows the sequestration of copper from albumin: a pathway to accumulation of copper in senile plaques. *Biochemistry* 52, 547–556.
- (13) Dickens, M. G., and Franz, K. J. (2010) A prochelator activated by hydrogen peroxide prevents metal-induced amyloid β aggregation. *ChemBioChem* 11, 59–62.
- (14) Cherny, R. A., Atwood, C. S., Xilinas, M. E., Gray, D. N., Jones, W. D., McLean, C. A., Barnham, K. J., Volitakis, I., Fraser, F. W., Kim, Y.-S., Huang, X., Goldstein, L. E., Moir, R. D., Lim, J. T., Beyreuther, K., Zheng, H., Tanzi, R. E., Masters, C. L., and Bush, A. I. (2001) Treatment with a Copper-Zinc Chelator Markedly and Rapidly Inhibits β -Amyloid Accumulation in Alzheimer's Disease Transgenic Mice. *Neuron* 30, 665–676.
- (15) Lannfelt, L., Blennow, K., Zetterberg, H., Batsman, S., Ames, D., Harrison, J., Masters, C. L., Targum, S., Bush, A. I., Murdoch, R., Wilson, J., and Ritchie, C. W. (2008) Safety, efficacy, and biomarker findings of PBT2 in targeting $A\beta$ as a modifying therapy for Alzheimer's disease: a phase IIa, double-blind, randomised, placebo-controlled trial. *Lancet Neurol.* 7, 779–786.
- (16) Adlard, P. A., Cherny, R. A., Finkelstein, D. I., Gautier, E., Robb, E., Cortes, M., Volitakis, I., Liu, X., Smith, J. P., Perez, K., Laughton, K., Li, Q.-X., Charman, S. A., Nicolazzo, J. A., Wilkins, S., Deleva, K., Lynch, T., Kok, G., Ritchie, C. W., Tanzi, R. E., Cappai, R., Masters, C. L., Barnham, K. J., and Bush, A. I. (2008) Rapid Restoration of Cognition in Alzheimer's Transgenic Mice with 8-Hydroxy Quinoline Analogs Is Associated with Decreased Interstitial $A\beta$. *Neuron* 59, 43–55.
- (17) Bareggi, S. R., and Cornelli, U. (2012) Clioquinol: Review of its Mechanisms of Action and Clinical Uses in Neurodegenerative Disorders. *CNS Neurosci. Ther.* 18, 41–46.
- (18) Ferraro, G., Massai, L., Messori, L., and Merlini, A. (2015) Cisplatin binding to human serum albumin: a structural study. *Chem. Commun.* 51, 9436–9439.
- (19) Yang, Y., Chen, T., Zhu, S., Gu, X., Jia, X., Lu, Y., and Zhu, L. (2015) Two macrocyclic polyamines as modulators of metal-mediated A[small beta]40 aggregation. *Integr. Biol.* 7, 655–662.
- (20) Stanyon, H. F., and Viles, J. H. (2012) Human Serum Albumin Can Regulate Amyloid-beta Peptide Fiber Growth in the Brain Interstitium: IMPLICATIONS FOR ALZHEIMER DISEASE. *J. Biol. Chem.* 287, 28163–28168.
- (21) Rocchi, A., Valensin, D., Aldinucci, C., Giani, G., Barbucci, R., Gaggelli, E., Kozlowski, H., and Valensin, G. (2012) NMR metabolomic investigation of astrocytes interacted with $A\beta$ 42 or its complexes with either copper(II) or zinc(II). *J. Inorg. Biochem.* 117, 326–333.
- (22) Roque, A., Sortino, R., Ventura, S., Ponte, I., and Suau, P. (2015) Histone H1 Favors Folding and Parallel Fibrillar Aggregation of the 1–42 Amyloid- β Peptide. *Langmuir* 31, 6782–6790.
- (23) Sadler, P. J., and Viles, J. H. (1996)) 1H and (113)Cd NMR Investigations of Cd(2+) and Zn(2+) Binding Sites on Serum Albumin: Competition with Ca(2+), Ni(2+), Cu(2+), and Zn(2+). *Inorg. Chem.* 35, 4490–4496.
- (24) Zhang, D., Li, H., and Wang, J.-B. (2015) Echinacoside inhibits amyloid fibrillization of HEWL and protects against $A\beta$ -induced neurotoxicity. *Int. J. Biol. Macromol.* 72, 243–253.
- (25) Camero, S., Ayuso, J. M., Barrantes, A., Benítez, M. J., and Jiménez, J. S. (2013) Specific Binding of DNA to Aggregated Forms of Alzheimer's Disease Amyloid Peptides. *Int. J. Biol. Macromol.* 55, 201–206.
- (26) Byeon, H. J., Min, S. Y., Kim, I., Lee, E. S., Oh, K. T., Shin, B. S., Lee, K. C., and Youn, Y. S. (2014) Human Serum Albumin-TRAIL Conjugate for the Treatment of Rheumatoid Arthritis. *Bioconjugate Chem.* 25, 2212–2221.
- (27) Xie, B., Dong, X., Wang, Y., and Sun, Y. (2015) Multifunctionality of Acidulated Serum Albumin on Inhibiting Zn(2+)-Mediated Amyloid beta-Protein Fibrillogenesis and Cytotoxicity. *Langmuir* 31, 7374–7380.
- (28) Xie, B., Li, X., Dong, X. Y., and Sun, Y. (2014) Insight into the inhibition effect of acidulated serum albumin on amyloid beta-protein fibrillogenesis and cytotoxicity. *Langmuir* 30, 9789–9796.
- (29) Nunes, A., Marques, S. M., Quintanova, C., Silva, D. F., Cardoso, S. M., Chaves, S., and Santos, M. A. (2013) Multifunctional iron-chelators with protective roles against neurodegenerative diseases. *Dalton T* 42, 6058–6073.
- (30) Khan, A., Ashcroft, A. E., Higenell, V., Korczak, O. V., and Exley, C. (2005) Metals accelerate the formation and direct the structure of amyloid fibrils of NAC. *J. Inorg. Biochem.* 99, 1920–1927.
- (31) Liao, Y. H., Chang, Y. J., Yoshiike, Y., Chang, Y. C., and Chen, Y. R. (2012) Negatively charged gold nanoparticles inhibit Alzheimer's amyloid-beta fibrillation, induce fibril dissociation, and mitigate neurotoxicity. *Small* 8, 3631–3639.
- (32) Dong, J., Shokes, J. E., Scott, R. A., and Lynn, D. G. (2006) Modulating amyloid self-assembly and fibril morphology with Zn(II). *J. Am. Chem. Soc.* 128, 3540–3542.
- (33) Ehrnhoefer, D. E., Bieschke, J., Boeddrich, A., Herbst, M., Masino, L., Lurz, R., Engemann, S., Pastore, A., and Wanker, E. E. (2008) EGCG redirects amyloidogenic polypeptides into unstructured, off-pathway oligomers. *Nat. Struct. Mol. Biol.* 15, 558–566.
- (34) Sharma, A. K., Kim, J., Prior, J. T., Hawco, N. J., Rath, N. P., Kim, J., and Mirica, L. M. (2014) Small Bifunctional Chelators That Do Not Disaggregate Amyloid beta Fibrils Exhibit Reduced Cellular Toxicity. *Inorg. Chem.* 53, 11367–11376.
- (35) Lauderback, C. M., Kanski, J., Hackett, J. M., Maeda, N., Kindy, M. S., and Butterfield, D. A. (2002) Apolipoprotein E modulates Alzheimer's $A\beta$ (1–42)-induced oxidative damage to synaptosomes in an allele-specific manner. *Brain Res.* 924, 90–97.
- (36) Du, X., Wang, Z., Zheng, Y., Li, H., Ni, J., and Liu, Q. (2014) Inhibitory effect of selenoprotein P on Cu(+)/Cu(2+)-induced Abeta42 aggregation and toxicity. *Inorg. Chem.* 53, 1672–1678.
- (37) Du, W. J., Guo, J. J., Gao, M. T., Hu, S. Q., Dong, X. Y., Han, Y. F., Liu, F. F., Jiang, S., and Sun, Y. (2015) Brazilin inhibits amyloid beta-protein fibrillogenesis, remodels amyloid fibrils and reduces amyloid cytotoxicity. *Sci. Rep.* 5, 7992.
- (38) Amir, A., Shmuel, E., Zagalsky, R., Sayer, A. H., Nadel, Y., and Fischer, B. (2012) Nucleoside-5'-phosphorothioate analogues are biocompatible antioxidants dissolving efficiently amyloid beta-metal ion aggregates. *Dalton. T.* 41, 8539–8549.

- (39) Wang, C., Wang, K., and Wang, Z. (2015) Development of gold nanoparticle based colorimetric method for quantitatively studying the inhibitors of Cu(2+)/Zn(2+) induced beta-amyloid peptide assembly. *Anal. Chim. Acta* 858, 42–48.
- (40) Wang, Z., Wang, Y., Wang, B., Li, W., Huang, L., and Li, X. (2015) Design, synthesis and evaluation of orally available clioquinol-moracin m hybrids as multi-target-directed ligands for cognitive improvement in a rat model of neurodegeneration in alzheimer's disease. *J. Med. Chem.* 58, 8616–8637.
- (41) Li, X., Wang, H., Lu, Z., Zheng, X., Ni, W., Zhu, J., Fu, Y., Lian, F., Zhang, N., Li, J., et al. (2016) Development of multifunctional pyrimidinylthiourea derivatives as potential anti-alzheimer agents. *J. Med. Chem.* 59, 8326–8344.
- (42) Chang, R., Knox, J., Chang, J., Derbedrossian, A., Vasilevko, V., Cribbs, D., Boado, R., Pardridge, W. M., and Sumbria, R. K. (2017) Blood–Brain Barrier Penetrating Biologic TNF- α Inhibitor for Alzheimer's Disease. *Mol. Pharmaceutics* 14, 2340–2349.
- (43) Chang, J., Jallouli, Y., Kroubi, M., Yuan, X. B., Feng, W., Kang, C. S., Pu, P. Y., and Betbeder, D. (2009) Characterization of endocytosis of transferrin-coated plga nanoparticles by the blood-brain barrier. *Int. J. Pharm.* 379, 285–292.
- (44) Wang, Q., Shah, N., Zhao, J., Wang, C., Zhao, C., Liu, L., Li, L., Zhou, F., and Zheng, J. (2011) Structural, morphological, and kinetic studies of β -amyloid peptide aggregation on self-assembled monolayers. *Phys. Chem. Chem. Phys.* 13, 15200–15210.
- (45) Khurana, R., Coleman, C., Ionescu-Zanetti, C., Carter, S. A., Krishna, V., Grover, R. K., Roy, R., and Singh, S. (2005) Mechanism of thioflavin T binding to amyloid fibrils. *J. Struct. Biol.* 151, 229–238.
- (46) Xie, B., Liu, F., Dong, X., Wang, Y., Liu, X. M., and Sun, Y. (2017) Modulation effect of acidulated human serum albumin on Cu2+-mediated amyloid β -protein aggregation and cytotoxicity under a mildly acidic condition. *J. Inorg. Biochem.* 171, 67–75.
- (47) Zhang, L., Yu, H., Zhao, X., Lin, X., Tan, C., Cao, G., and Wang, Z. (2010) Neuroprotective effects of salidroside against beta-amyloid-induced oxidative stress in SH-SY5Y human neuroblastoma cells. *Neurochem. Int.* 57, 547–555.
- (48) Keller, J. N., Lauderback, C. M., Butterfield, D. A., Kindy, M. S., Yu, J., and Markesberry, W. R. (2000) Amyloid β -Peptide Effects on Synaptosomes from Apolipoprotein E-Deficient Mice. *J. Neurochem.* 74, 1579–1586.
- (49) Noy, D., Solomonov, I., Sinkevich, O., Arad, T., Kjaer, K., and Sagi, I. (2008) Zinc-Amyloid β Interactions on a Millisecond Time-Scale Stabilize Non-fibrillar Alzheimer-Related Species. *J. Am. Chem. Soc.* 130, 1376–1383.
- (50) Schägger, H. (2006) Tricine-SDS-PAGE. *Nat. Protoc.* 1, 16.